Nuclear quantum effects in solid water: new insights from computational modeling

Rasti, S.

CHAPTER 6

Volume Isotope Effect of Ice Ih

This chapter is based on:

S. Rasti, E. Ö. Jónsson, H. Jónsson and J. Meyer, New Insights into the Volume Isotope Effect of Ice Ih from polarizable many-body Potentials, *to be submitted*

Abstract

The volume-isotope effect (VIE) of ice Ih is studied computationally. Nuclear quantum effects in the Helmholtz free energy are accounted for based on the quasi-harmonic approximation and evaluated by extensive phonon calculations. Focusing on recently developed polarizable many-body potentials as interaction models, one of them (MB-pol) is found to yield the anomalous VIE in very good agreement with the most recent high-resolution neutron diffraction measurements – much better than DFT calculations with the PBE functional. Using the MB-pol energy partitioning, a surprisingly large influence of the cooperative interaction between three water molecules for the VIE and its temperature dependence up to 200 K is being revealed. The interaction models are further scrutinized by decomposing the zero-point pressure into contributions from different vibrational mode groups. MB-pol's remarkable performance is confirmed by comparing to a hitherto unconsidered benchmark value for the intramolecular stretching modes of H_2O ice Ih obtained from Raman spectroscopy data. This unveils the delicate competition between the librational and intramolecular stretching modes upon substitution of hydrogen by deuterium as the driving force behind the VIE – mitigated by three-body effects.

6.1 Introduction

Nuclear quantum effects can manifest themselves quite prominently in macroscopic thermodynamic properties, like for example phase transition enthalpies [1], negative thermal expansion (NTE) or density change at low temperatures upon substitution of a light by a heavier isotope [2]. The latter is called the volume isotope effect (VIE) and originates from the zero-point energy of the lattice vibrations (phonons). Most materials show a normal VIE, which means substitution with heavier isotopes results in a smaller volume per unit cell at temperatures approaching the absolute zero. A hand-waving rationalization in a classical picture is that the larger vibrational amplitude and concomitant volume ascribed to a lighter isotope compared to heavier isotope, which

both experience the same chemical interaction potential at the same temperature. In ice Ih, the most common form of solid water on earth, the VIE is anomalous, resulting in a smaller unit cell volume of the H_2O compared to the D_2O isotopologue (about 0.1 % up to 200 K [3, 4]). Despite its small magnitude, the effect has been very well quantified experimentally. Only recently, high-resolution neutron diffraction measurements [4] have reduced the uncertainties for the unit cell volumes of ice Ih compared to earlier work [3] over a wide temperature range and thus provide an excellent benchmark for atomistic interaction models that can be employed in computational studies.

Computational modeling of the VIE is very challenging. So far, water force fields ranging from simple fixed point charge up to sophisticated polarizable models have all predicted a normal VIE for ice Ih [5–7]. Density functional theory on the other hand is able to model the VIE of different ice phases [7–9]. However, even a qualitatively correct description depends very strongly on the computational settings, in particular the choice of the exchange-correlation functional [7]. Quantification of the VIE using embedded-fragment ab initio second-order many-body perturbation (MP2) theory has been faring somewhat better [10]. But also here, the results are very sensitive to computational details like the basis set size and the embedding field. This also holds for the individual contributions of the different groups of phonon modes to the zero-point pressure, which are ultimately responsible for the VIE [8, 10]. These contributions are commonly expressed in form of the mode-specific Grüneisen parameters and have not been benchmarked against experimental data. Consequently, a detailed understanding of the VIE's origin in terms of the competition of different contributions to the chemical interaction potential has been elusive so far.

In this work, that understanding is provided based on recently developed polarizable many-body potentials as interaction models. Building on recent studies (see Chapters 3 and 5), the quasi-harmonic approximation is employed to account for nuclear quantum effects in the Helmholtz free energy by means of extensive phonon calculations. The MB-pol interaction model, whose short-range part is rooted in coupled-cluster calculations, yields the anomalous VIE of ice Ih in better agreement with the experimental

reference value than DFT calculations with the PBE functional. A decomposition of the zero-point pressure into contributions from different vibrational mode groups together with a hitherto unconsidered benchmark value obtained from Raman spectroscopy [11] allows to scrutinize this further. According to the MB-pol total energy parititioning, the delicate competition between the librational and intramolecular stretching modes driven by a surprisingly large influence of three-body effects is responsible for the anomalous VIE of ice Ih.

6.2 Methods

For the quantification of the VIE, this work employs the quasi-harmonnic approximation (QHA), which has been used successfully for the same purpose in the past [7–10, 12]. According to the QHA, the Helmholtz free energy of the ice crystal is given by

$$F(V,T) = U(V) \; + \; \underbrace{\frac{1}{2}\sum_i \hbar\omega_i(V)}_{E_{\mathrm{ZP}}(V)} \; + k_{\mathrm{B}}T \sum_i \ln\left(1 - \exp\left(\frac{-\hbar\omega_i(V)}{k_{\mathrm{B}}T}\right)\right) \qquad (6.1)$$

and is conveniently evaluated per molecule. U is the internal energy that describes the interaction between molecules in the crystal. ω_i are the vibrational modes, which determine the second (zero-point energy E_{zp}) and temperature-dependent third term of F. For the sake of simplicity, they are denoted by a collective index i that stands for both wave-vector and band indices of the corresponding phonon modes (see Section 2.4 for more details). The internal energy U and the vibrational modes ω_i depend on the unit cell volume V, so that the minimum of F with respect to V at a given temperature is generally different for H_2O and D_2O isotopologues. The corresponding volumes are labeled $V_{\mathrm{H_2O}}(T)$ and $V_{\mathrm{D_2O}}(T)$ in the following. V_0 minimizes $U(V)$, with the zero-reference of the latter defined such that the lattice energy $E_{\mathrm{lat}} = U(V_0)$.

In this work, calculations with different interaction models are performed[1], employing and extending the Atomic Simulation Environment (ASE) [13] for interfacing

[1] More details about these models are given in Sections 2.2 and 2.3 of this thesis.

their respective implementations. This includes the fixed-point-charges-based force fields q-TIP4P/F [14, 15] (as available in LAMMPS [16]), the polarizable force fields AMOEBA14 [17, 18] (as implemented in TINKER [19]), SCME/f [20] (and Chapter 5) and MB-pol (as implemented in the MBX package) [21–23]. All-electron density functional theory (DFT) calculations with the PBE exchange-correlation functional [24] are carried out with FHI-aims code [25, 26], using the same high-accuracy settings thoroughly verified [27] and employed [28, 29] for ice Ih in previous work (see Section 6.A.1 for details). The DFT calculations mimic proton disorder with a simulation cell containing 12 molecules [30]. A 96 molecule cell or supercells of this cell have been used for the force field interaction models to ensure the same level of convergence for V_0 ($\pm 0.01\,\text{Å}^3$ per molecule [27]). For all interaction models, V_0 is calculated with ASE as in our earlier work by a combined optimization of the cell vectors and the molecular degrees of freedom preserving the space group [29] with a maximum force threshold of $1.0 \times 10^{-3}\,\text{eV Å}^{-1}$.

A continuous representation of $U(V)$ is obtained by least-square fitting to the Rose-Vinet [31] equation of state. Isotropic contraction and expansion of V_0 by $\pm 4\,\%$ yields 11 structures for each interaction model, for which again all molecular degrees of freedoms have been relaxed. Phonon calculations have been carried out for all of these structures with the PHONOPY code [32], using a finite displacement [33] of 0.02 Å in $3 \times 3 \times 3$ supercells of the original simulation cell. The Brillouin zone has been sampled by $30 \times 30 \times 30$ and $10 \times 10 \times 10$ grids of phonon wave vectors in the 12 molecule and 96 molecule simulation cells, respectively. The implementation of the QHA in PHONOPY then yields a continuous representation of the volume-dependent second and third terms in Eq. (6.1) and thus $V_{\text{H}_2\text{O}}(T)$, $V_{\text{D}_2\text{O}}(T)$, $\text{VIE}(T) = \frac{V_{\text{D}_2\text{O}}}{V_{\text{H}_2\text{O}}} - 1$[2] and the phonon mode-dependent Grüneisen parameters γ_i. Convergence checks for the VIE can be

[2]This work uses the same convention as in the recent work Fortes [4] to quantify the volume isotope effect, i.e., $\text{VIE} = \frac{V_{\text{D}_2\text{O}} - V_{\text{H}_2\text{O}}}{V_{\text{H}_2\text{O}}}$, whereas others have used $\text{VIE'} = \frac{V_{\text{H}_2\text{O}} - V_{\text{D}_2\text{O}}}{V_{\text{D}_2\text{O}}}$, which leads to almost the same absolute numbers but flips the sign. Both expressions are related according to $\text{VIE} = -\frac{\text{VIE'}}{1+\text{VIE'}}$ and $\text{VIE'} = -\frac{\text{VIE}}{1+\text{VIE}}$, respectively. For the sake of brevity, the temperature dependence has been omitted.

found in Section 6.A.2.

6.3 Results and Discussion

Table 6.1 compiles experimental data and results from calculations for V_0, V_{H_2O}, V_{D_2O} and the VIE for ice Ih. A positive (negative) value corresponds to an anomalous (normal) VIE. The most recent results from the high-resolution neutron diffraction measurements by Fortes [4] yield an even smaller and more accurately determined anomalous VIE ($+0.050 \pm 0.002\,\%$) than the earlier data from the work of Röttger *et al.* [3] ($+0.090 \pm 0.015\,\%$). In both studies, the lowest temperature at which measurements have been performed is 10 K. For that reason, we have calculated V_{H_2O} and V_{D_2O} at both 0 and 10 K to confirm that this has no effect on any of the numbers presented in Table 6.1. As demonstrated only recently, errors related to the treatment of core and valence electrons in different DFT codes can be sizeable for the calculation of energy-volume curves $U(V)$ [34] and could thus significantly affect results for the VIE. This is the most likely reason for the difference of 0.07 % between earlier DFT results obtained with the same exchange-correlation functional (PBE) [7, 12]. Our own PBE calculations eliminate this source of error and perfectly reproduce the value for V_0 obtained in earlier work [27, 28]. In combination with our meticulous convergence tests for the phonon calculations with respect to the VIE (see Section 6.A.2), we can therefore confirm without any further doubts the conclusions from earlier work [7, 12], namely that the PBE functional reproduces the experimentally observed anomalous VIE but overestimates it. Likewise, our computational setup also confirms that the q-TIP4P/F force field, which is based on fixed point charges (see Section 2.3.1) yields a normal VIE for ice Ih [7]. The same holds for the two polarizable force fields AMOEBA14 and the recently established SCME/f (see Chapter 5). The results for V_{H_2O} and also for V_{D_2O} obtained with SCME/f show the best agreement with the experimental values. SCME/f is followed by MB-pol, which also yields $V_{H_2O} < V_{D_2O}$ and consequently a correct description of the anomalous VIE. The absolute value of +0.14 % is even in much better agreement with the experimental data than (our) PBE results. This re-

Table 6.1: Volumes V_0, V_{H_2O} and V_{D_2O} for ice Ih (in $Å^3$ per molecule, rounded to two decimals). The volume isotope effect is quantified by VIE $= \frac{V_{D_2O}}{V_{H_2O}} - 1$ (in percent, calculated using more decimals). The experimental data for V_{H_2O}, V_{D_2O} and VIE have been measured at $T = 10\,K$ [3, 4]. Calculations from this work with all interaction models at 0 and 10 K do not yield any differences in the second decimal.

	V_0	V_{H_2O}	V_{D_2O}	VIE
Experiments				
Fortes [4]		32.06	32.07	+0.05
Röttger *et al.* [3]		32.05	32.08	+0.09
Calculations – DFT with PBE functional[a]				
this work	30.78	31.03	31.14	+0.36
Pamuk *et al.* [7][b]	29.98	30.09	30.19	+0.33
Murray and Galli [12]	30.50	30.57	30.67	+0.40
Calculations – polarizable force fields				
MB-pol	31.07	31.44	31.49	+0.14
MB-pol w/o 3B	29.14	30.18	30.06	−0.39
SCME/f	30.38	31.98	31.68	−0.90
AMOEBA14	31.82	33.35	33.12	−0.67
Calculations – fixed-charge force field				
q-TIP4P/F[c]	31.24	32.83	32.63	−0.61

[a] See Section 6.A.1 in the appendix to this chapter for a collection of other values for V_0 obtained with the PBE exchange-correlation functional in previous work.

[b] Value obtained with the QHA and a k-mesh of 729 points, which is most comparable to the present work.

[c] Note that these values differ slightly from the results obtained by Pamuk *et al.* [7] due to differences in the computational setups.

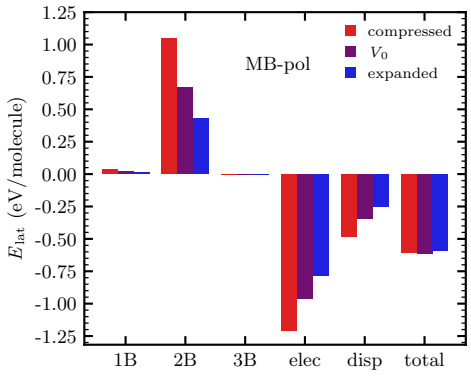

Figure 6.1: Lattice energy E_{lat} and its contributions according to the total energy decomposition of the MB-pol force field [21, 22, 35] (all in eV per molecule). The intramolecular (1B) as well as intermolecular short-range two-body (2B), three-body (3B) electrostatic (elec) and dispersion (disp) contributions add up to E_{lat} (total). Violet, red and blue bars depict equilibrium (V_0) and isotropically compressed ($0.96 \cdot V_0$) and expanded ($1.04 \cdot V_0$) lattice configurations, respectively, as encountered during the phonon calculations for the determination of the VIE according to the QHA.

markable result also bares the opportunity to better understand what contributions to the chemical bonding in the ice Ih crystal are responsible for the VIE. Among all the force fields considered here, MB-pol is the only one which explicitly accounts for short-range interactions involving triples of water molecules, which have been parameterized to quantum-chemical CCSD(T) calculations [21] (see also Section 2.3.4). Indeed, omitting these terms (MB-pol w/o 3B in Table 6.1) yields a normal VIE.

At first glance, the strong influence of these terms is surprising, because they do not constitute a large contribution to the cohesive (lattice) energy according to the decomposition of the internal energy at the equilibrium volume $U(V_0)$ in the MB-pol force field [36]. This does not change when moving away from V_0 as shown in Fig. 6.1. Compression of the ice Ih lattice leads to an increase of the repulsive short-range interactions between pairs of water molecules (two-body terms), which is almost compensated by the increase of the long-range electrostatic and dispersion contributions. The opposite

holds when expanding the volume. The one-body (i.e., deformation of individual water molecules) and three-body terms play hardly any role.[3]

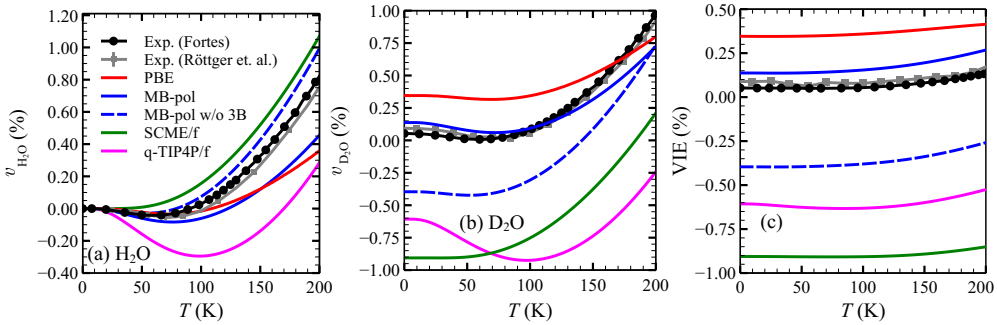

Figure 6.2: Relative volume changes (a) $v_{\mathrm{H_2O}}(T) = \frac{V_{\mathrm{H_2O}}(T)}{V_{\mathrm{H_2O}}} - 1$ and (b) $v_{\mathrm{D_2O}}(T) = \frac{V_{\mathrm{D_2O}}(T)}{V_{\mathrm{H_2O}}} - 1$ of ice Ih, both with respect to $V_{\mathrm{H_2O}}$ from Table 6.1 for the same interaction models except AMOEBA14. (c) shows the resulting temperature dependence of the volume isotope effect $\mathrm{VIE}(T) = \frac{V_{\mathrm{D_2O}}(T)}{V_{\mathrm{H_2O}}(T)} - 1 = \frac{v_{\mathrm{D_2O}}(T)+1}{v_{\mathrm{H_2O}}(T)+1} - 1$. Error indicators for the experimental data from Röttger *et al.* [3] (gray) are hardly visible, and even less so for the data from Fortes [4] (black), whereby lines are meant to guide the eye.

To investigate the importance of the three-body contributions (in MB-pol) for the VIE more closely, it is instructive to evaluate $V_{\mathrm{H_2O}}$ and $V_{\mathrm{D_2O}}$ over a wider range of temperatures, which has recently been remeasured with higher accuracy by Fortes [4] as well. This is illsutrated in form of the relative volume changes $v_{\mathrm{H_2O}}(T)$ and $v_{\mathrm{D_2O}}(T)$ up to $T \leq 200\,\mathrm{K}$ in Fig. 6.2(a) and Fig. 6.2(b), respectively. The experimental data for H_2O and D_2O ice Ih shows a negative slope for $T \leq 70\,\mathrm{K}$. This negative thermal expansion (NTE) has been modeled successfully before [10, 37] and is also reproduced by all methods considered here, except for SCME/f. This leads to a small offset in the relative volume change for H_2O between SCME/f and the experimental data at higher temperatures, which remains almost constant. Apart from that, SCME/f captures the shape of the experimental curve for $v_{\mathrm{H_2O}}(T)$ very well, i.e. better than any other

[3]Because polarizability is accounted for in MB-pol, the electrostatics are long-range many-body interactions, see Section 2.3.4.

method considered here (except for MB-pol w/o 3B). MB-pol yields a slightly worse description of $v_{H_2O}(T)$ similar to PBE. For $v_{D_2O}(T)$ on the other hand, it provides by far the best possible description of the relative volume change (followed by PBE). Consequently, MB-pol also provides the best possible description of the VIE over the entire temperature range considered here. Not including the three-body effects in MB-pol improves the shape of $v_{H_2O}(T)$ but significantly worsens results for VIE(T), resulting in the prediction of a normal volume isotope effect. Both SCME/f and q-TIP4P/f yield an even worse shape for $v_{H_2O}(T)$ compared to the experimental data. q-TIP4P/f describes a too strong NTE over a too large temperature interval ($T \leq 100\,\mathrm{K}$) for both H_2O and D_2O, error canceling ultimately results in a better description of VIE(T) compared to SCME/f.

According to the QHA (see Eq. (6.1)) the temperature dependence of the equilibrium volume is completely determined by the vibrational modes. As demonstrated in previous work [5, 7, 8, 10], their change upon compression and expansion can be analyzed in detail by means of the mode-dependent Grüneisen parameters $\gamma_i = -\frac{V}{\omega_i}\frac{\partial \omega_i}{\partial V}$, which define the zero-point pressure

$$P_{\mathrm{ZP}} = -\frac{\partial E_{\mathrm{ZP}}}{\partial V} = -\frac{\hbar}{2V}\sum_i \frac{\partial \omega_i}{\partial V} = \frac{\hbar}{2V}\sum_i \omega_i \gamma_i \quad . \tag{6.2}$$

Positive (negative) values for P_{ZP} yield expansion (contraction) of the volume due to zero-point energy effects.[4] Figure 6.3(a) and (b) show that all methods yield a positive total zero-point pressure for both H_2O or D_2O, respectively, as to be expected according to the results compiled in Table 6.1. For an anomalous (normal) VIE (at 0 K), the total P_{ZP} needs to be smaller (larger) for H_2O than for D_2O. The corresponding differences are shown in Fig. 6.3(c), and indeed only for PBE and MB-pol comes out $P_{\mathrm{ZP}}^{H_2O} - P_{\mathrm{ZP}}^{D_2O} < 0$. Figure 6.3 also shows a decomposition of the zero-point pressure into contributions from the five different vibrational mode groups characterized by hydrogen-bond bending (HB) and stretching (HS), librations (L), intramolecular bending (B) and stretching (S). Unlike the differences of the total P_{ZP}, which unfor-

[4] P_{ZP} is an intensive quantity. For its proper evaluation in practical calculations, $\frac{\partial E_{\mathrm{ZP}}}{\partial V}$ must be evaluated for the same reference volume as $U(V)$, i.e., per molecule in this work.

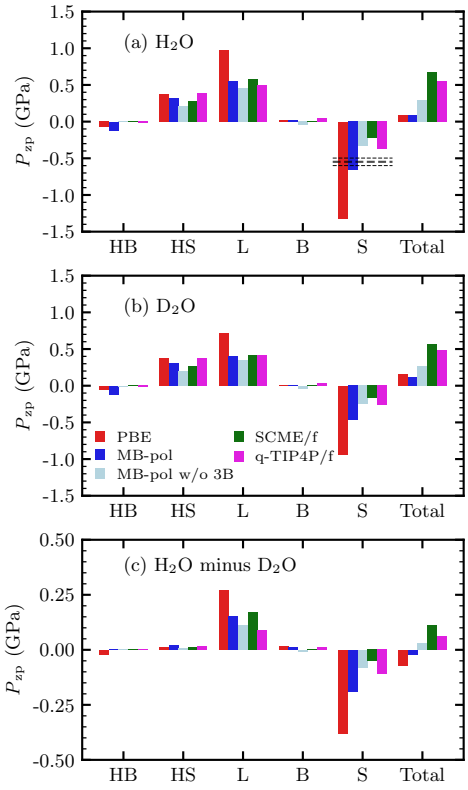

Figure 6.3: Total zero-point pressure P_{ZP} (rightmost bars) and its decomposition according to Eq. (6.2) into the vibrational mode groups comprised of hydrogen-bond bending (HB, 0 to 125 cm^{-1}), hydrogen-bond stretching (HS, 125 to 500 cm^{-1}), librations (L, 500 to 1500 cm^{-1} (425 to 900 cm^{-1}) in H_2O (D_2O) ice Ih), intramolecular bending (B, 1500 to 2000 cm^{-1} (900 to 1300 cm^{-1}) in H_2O (D_2O) ice Ih) and intramolecular stretching (S, 3000 to 4000 cm^{-1} (2000 to 3000 cm^{-1}) in H_2O (D_2O) ice Ih) modes in (a) H_2O and (b) D_2O) ice Ih. Results are shown using the same interaction models as in Fig. 6.2. Panel (c) illustrates the differences between (a) and (b) ($P_{\mathrm{ZP}}(H_2O) - P_{\mathrm{ZP}}(D_2O)$). An estimate for $P_{\mathrm{ZP}}^{\mathrm{S}}$ based on experimental data for H_2O ice Ih is indicated in panel (a) (see text and Section 6.A.3 for details).

tunately cannot be measured directly, the differences between the contributions from the mode groups vary much more when considering different interaction models. The P_{ZP} contribution from the HB and HS groups is hardly affected by H-D substitution (see Fig. 6.3)(c)), which is not surprising because both of these mode groups involve the frustrated translation of entire H_2O and D_2O molecules. Likewise, all methods suggest that the B modes contribute very little to the VIE, and that it is the delicate balance between the expansive P_{ZP} of the L modes (frustrated rotations) and the contractive P_{ZP} of the S modes, which predominantly determine the sign of the zero-point pressures difference between both isotopologues.

Salim *et al.* [10] have already pointed that the subtle interplay of the P_{zp} contributions from different mode groups makes it additionally challenging to determine whether a particular interaction model captures the VIE correctly and for the right reason. We have already noted in our earlier work [29] that the measurements by Minceva-Sukarova *et al.* [11] of the pressure dependence of the Raman peak for the S mode group in H_2O ice Ih at 246 K play a key role in this context. As further detailed in Section 6.A.3, this allows us to obtain a good estimate for the contribution by the S mode group $P_{\mathrm{zp}}^{\mathrm{S}} \approx -0.548 \pm 0.051\,\mathrm{GPa}$, which is based on experimental data alone. Fig. 6.3(a) includes this value as black horizontal line. Considering that error estimates are lower bounds, MB-pol almost reproduces this value exactly ($-0.66\,\mathrm{GPa}$) and clearly comes much closer than PBE ($-1.32\,\mathrm{GPa}$) and MB-pol w/o 3B ($-0.33\,\mathrm{GPa}$). This confirms that three-body effects play indeed a very important role for the correct atomistic description of the VIE.

Unfortunately, Minceva-Sukarova *et al.* [11] have not measured the S mode group frequency shift for the D_2O isotopologue of ice Ih. Since all interaction models suggest a strongly localized character of the S modes, the outcome of such a measurement can be estimated based on the reduced masses associated with the O−H and O−D bonds as $0.728 \cdot P_{\mathrm{zp}}^{\mathrm{S}} \approx -0.399\,\mathrm{GPa}$ (see Section 6.A.3), which is consequently again excellent agreement with the MB-pol value in Fig. 6.3(b) ($-0.47\,\mathrm{GPa}$). While it would be good to see this value confirmed in future experiments, the outstanding performance of MB-

pol and the concomitant understanding would be better scrutinized by experimental data for the L modes. Ideally, such data could also be measured at temperatures much lower than 246 K, to avoid systematic errors related to mode softening effects in future comparisons of experiments and theory.

6.4 Conclusion and Outlook

In summary, this study provides new insights into the volume isotope effect of ice Ih based on calculations within the quasi-harmonic approximation by employing a variety of different interaction models. All-electron DFT calculations with the PBE exchange-correlation functional provide a reference value and confirm that PBE yields an anomalous VIE but largely overestimates its magnitude. Among the three state-of-the-art polarizable force fields only MB-pol yields an anomalous VIE the magnitude of which is in significantly better agreement with the most recent experimental data than PBE. A detailed analysis based on the MB-pol energy partitioning reveals a surprisingly large influence of the cooperative interaction between three water molecules for the VIE and the temperature dependence of the volume of H_2O and D_2O ice Ih up to 200 K. Finally, the zero-point pressure is decomposed into contributions from different vibrational mode groups, and an estimate from experimental data for the contribution from the intramolecular stretching modes of H_2O ice Ih is extracted, which is completely independent from all measurements related to the VIE. Among all interaction models considered here, this is in best agreement with MB-pol – while being significantly overestimated by PBE and underestimated by all other force fields. This suggests that MB-pol yields the anomalous VIE of ice Ih for the right reason. It thus also enables unprecedented quantification and atomic-scale understanding of its driving force, namely the delicate competition between the expansive librational and contractive intramolecular stretching modes upon substitution of hydrogen by deuterium, mitigated by three-body effects. Future computational studies should investigate other ice polymorphs. However, before embarking on this endeavor, it would be highly desirable to have experimental benchmark data for contribution from other vibrational

mode groups to the zero-point pressure, ideally with smaller error bars and for both H_2O and D_2O isotoplogues. This bares the exciting prospect of obtaining fundamental insights about volume isotope effects in those other polymorphs as well, and to establish a delicate benchmark that can be used for the further development of interaction models targeting condensed forms of water.

6.A Appendix

6.A.1 Comparison to Previous DFT Calculations

Table 6.2: Volumes V_0 for ice Ih (see main text for definition) as obtained "directly" from DFT calculations (i.e., without considering ZPE effects) with the PBE exchange-correlation functional. Results from this work, Pamuk *et al.* [7] and [12] are already given in Table 6.1. Equivalent results for ice VIII are shown to further illustrate difference between all-electron calculations and those which employ approximations for core and valence electrons. All values are in $Å^3$ per molecule.

	V_0(ice Ih)	V_0(ice VIII)
all-electron calculations		
this work	30.78	20.73
Santra *et al.* [27] and Sun *et al.* [28]	30.79	20.74
calculations with approximations for core and valence electrons		
Pamuk *et al.* [7]	29.98	
Murray and Galli [12]	30.50	20.44
Umemoto and Wentzcovitch [38]		20.12
Feibelman [39]	30.65	
Brandenburg *et al.* [40]	30.15	20.36
Liu and Ojamäe [41]	30.3	20.5

All DFT calculations in this work employ the PBE exchange-correlation functional [24]. They have been carried out the with the all-electron DFT code FHI-aims [25,

26], which employs numerically tabulated atom-centered orbitals as basis set. The standard tight settings and tier-2 and tier-3 basis sets for hydrogen and oxygen atoms, respectively. A $4 \times 4 \times 4$ Monkhorst-Pack grid [42] is employed for Brillouin zone sampling. These settings are the same as those established by Santra *et al.* [27], whose thorough convergence tests gave an estimate of $\pm 0.01\,\text{Å}^3$ for the numerical accuracy of V_0 with respect to these settings. Sun *et al.* [28] have used the same settings afterwards, As to be expected and shown in Table 6.2, all three calculations agree perfectly within the aforementioned accuracy margin.

Table 6.2 also reveals that DFT-PBE calculations with approximations for the treatment of core and valence electrons (pseudopotentials) systematically underestimate V_0 for both ice Ih and ice VIII. A more detailed investigation of this interesting finding is outside the scope of this work.

6.A.2 Convergence Tests for the VIE Calculations

Three sets of convergence tests have been carried out, to scrutinize the accuracy of the results reported in Table 6.1 for $V_{\text{H}_2\text{O}}$ and $V_{\text{D}_2\text{O}}$ (and thus VIE) with respect to the following three parameters:

1. Accuracy of geometry optimization for the water molecules in the simulation cell. This is quantified by the force threshold F_{max} criterion that is used to stop the relaxation. Smaller values for F_{max} yield for accurate results.

2. Finite displacement in phonon calculations Δ_{disp}. For force fields where analytic formulations of forces are available, smaller values of Δ_{disp} reduce the error for the second derivatives in the phonon calculations. However, in DFT calculations, forces (usually) come with a numerical error, the reduction of which requires additional computational effort (i.e., increasing the accuracy of the self-conistent field cycle). Therefore, a small value that is as large as possible not to affect $V_{\text{H}_2\text{O}}$ and $V_{\text{D}_2\text{O}}$ (and thus VIE) is sought after here.

3. Range of isotropic contraction and expansion of V_0 used for the construction

of a continuous representation of the volume-dependent terms required for the quasi-harmonic approximation (QHA) given by Eq. (6.1). Different intervals $[(1 - s_{\max})V_0; (1 + s_{\max})V_0]$ have been considered, which are all discretized by 11 equidistant points. For too small intervals the numerical noise in the volumes gains a too large influence on the fit, while too large intervals leave the regime of validity for the QHA.

For reasons of computational convenience, all calculations for these convergence tests have been carried with the AMOEBA14 force field. All the results are compile in Table 6.3. Accurate results can be obtained with $F_{\max} = 10^{-3}\,\mathrm{eV\,\AA^{-1}}$, $\Delta_{\mathrm{disp}} = 0.02\,\mathrm{\AA}$ and $s_{\max} = 4\,\%$. As described in the main text, this is what has been used for all interaction models throughout this work.

6.A.3 Zero-point Pressures from Experimental Data

Using Raman spectroscopy Minceva-Sukarova *et al.* [11] measured the shift of the intramolecular stretching mode peak in the H_2O-isotopologue of ice Ih at 246 K when applying external pressure

$$\frac{\partial \nu_{\mathrm{S}}}{\partial P} = -78.0 \pm 7.2\,\mathrm{cm^{-1}\,GPa^{-1}} \quad , \tag{6.3}$$

which yields

$$h\frac{\partial \nu_{\mathrm{S}}}{\partial P} = 1.549 \pm 0.143 \times 10^{-21}\,\mathrm{J\,GPa^{-1}} \tag{6.4}$$

($1\,h\,\mathrm{cm^{-1}} = 1.9863 \times 10^{-23}\,\mathrm{J}$). This allows us to obtain an estimate based on experimental data for the zero-point pressure of the intramolecular stretching mode group

$$P_{\mathrm{zp}}^{\mathrm{S}} \approx -\sum_{i\in \mathrm{S}} \frac{\hbar}{2}\frac{\partial \omega_i}{\partial V} = \frac{1}{2}\frac{B_0}{V_0}\,h\sum_{i\in \mathrm{S}}\frac{\partial \nu_i}{\partial P} \quad , \tag{6.5}$$

where $\frac{\partial \omega}{\partial V} = \frac{\partial P}{\partial V}\frac{\partial \omega}{\partial P} = -2\pi\frac{B_0}{V_0}\frac{\partial \nu}{\partial P}$. In the following, it is assumed that $\frac{\partial \nu_{\mathrm{S}}}{\partial P}$ does not change significantly with temperature.

The highly accurate experimental values for the bulk modulus $B_0 = 11.33\,\mathrm{GPa}$ (extrapolated to 0 K) [43] and the unit cell volume $V_0 = 32.05\,\mathrm{\AA^3}$ per H_2O molecule [4]

Table 6.3: Results of convergence tests with respect to the three parameters $F_{\max}$, Δ_{disp} and $s_{\max}$ as defined in the text. Note that the volumes V_{H_2O} and V_{D_2O} (for ice Ih) are rounded to two decimals, and that VIE $= \frac{V_{D_2O}}{V_{H_2O}} - 1$ is calculated using more decimals.

$F_{\max}$ (eV Å^{-1})	Δ_{disp} (Å)	$s_{\max}$ (%)	V_{H_2O} (Å^3/H_2O)	V_{D_2O} (Å^3/D_2O)	VIE (%)
Force threshold criterion for geometry optimizations					
1.0×10^{-4}	0.02	4.0	33.35	33.12	−0.67
1.0×10^{-3}	0.02	4.0	33.35	33.12	−0.67
2.5×10^{-3}	0.02	4.0	33.36	33.12	−0.69
5.0×10^{-3}	0.02	4.0	33.37	33.13	−0.69
Finite displacement for phonon calculations					
1.0×10^{-3}	0.01	4.0	33.35	33.12	−0.67
1.0×10^{-3}	0.02	4.0	33.35	33.12	−0.67
1.0×10^{-3}	0.03	4.0	33.36	33.12	−0.68
1.0×10^{-3}	0.06	4.0	33.37	33.13	−0.68
1.0×10^{-3}	0.08	4.0	33.38	33.14	−0.69
Maximum expansion and contraction of cell volume for the QHA					
1.0×10^{-3}	0.02	0.2	33.23	33.02	−0.60
1.0×10^{-3}	0.02	0.5	33.21	33.02	−0.56
1.0×10^{-3}	0.02	1.0	33.26	33.07	−0.54
1.0×10^{-3}	0.02	2.0	33.29	33.10	−0.60
1.0×10^{-3}	0.02	3.0	33.33	33.11	−0.68
1.0×10^{-3}	0.02	4.0	33.35	33.12	−0.67
1.0×10^{-3}	0.02	5.0	33.35	33.12	−0.67

(at 10 K), result in

$$\frac{1}{2}\frac{B_0}{V_0} = 0.177\,\mathrm{GPa\,\AA^{-3}} \quad . \tag{6.6}$$

Assuming the same shift for both symmetric and antisymmetric stretching modes and neglecting dispersion ($\frac{\partial \nu_i}{\partial P} = \frac{\partial \nu_\mathrm{S}}{\partial P}$), which is consistent with the Raman experiments of Minceva-Sukarova *et al.* [11][5], result in

$$h \sum_{i \in \mathrm{S}} \frac{\partial \nu_i}{\partial P} \approx 2 \cdot h \frac{\partial \nu_\mathrm{S}}{\partial P} \approx -3.099 \pm 0.286 \times 10^{-21}\,\mathrm{J\,GPa^{-1}} \tag{6.7}$$

where the factor of two comes from the summation over both stretching modes per molecule. This leads to the final value

$$P_\mathrm{zp}^\mathrm{S} \approx -0.548 \pm 0.051\,\mathrm{GPa} \tag{6.8}$$

($1\,\mathrm{J\,\AA^{-3}} = 10^{30}\,\mathrm{Pa}$). Due to aforementioned approximations, the indicated errors should be considered as lower bounds.

Unfortunately, Minceva-Sukarova *et al.* [11] do not report $\frac{\partial \nu_\mathrm{S}}{\partial P}$ for D_2O ice Ih, and to the best of our knowledge no such measurement is available. Despite the relatively strong hydrogen bonding in ice Ih [44], the S modes are still largely dominated by the local intramolecular potential along a single O−H bond. This leads to a simple one-dimensional picture, where the relative shift of the corresponding O−D stretching mode is (approximately) given by

$$\alpha = \frac{\nu_\mathrm{S}^{\mathrm{D_2O}}}{\nu_\mathrm{S}^{\mathrm{H_2O}}} \approx \frac{\mu_{\mathrm{O-H}}}{\mu_{\mathrm{O-D}}} = \sqrt{\frac{m_\mathrm{H}}{m_\mathrm{D}}\frac{m_\mathrm{O}+m_\mathrm{D}}{m_\mathrm{O}+m_\mathrm{H}}} \approx 0.728 \quad , \tag{6.9}$$

where $\mu_{\mathrm{O-X}} = \frac{m_\mathrm{X} \cdot m_\mathrm{O}}{m_\mathrm{X}+m_\mathrm{O}}$ ($\mathrm{X} \in \{\mathrm{H}, \mathrm{D}\}$) is the reduced mass of the corresponding O−X bond with $m_\mathrm{H} = 1.0078\,\mathrm{u}$, $m_\mathrm{D} = 2.0141\,\mathrm{u}$, $m_\mathrm{O} = 15.999\,\mathrm{u}$. The calculations with all interaction models considered in this work leads to values between 0.726 and 0.730 for α, which confirms that deviations from this one-dimensional picture are very small. In fact, Minceva-Sukarova *et al.* [11] do provide the average stretching mode for both H_2O ($\nu_{\mathrm{OH}(\mathrm{H_2O})} = 3138\,\mathrm{cm^{-1}}$) and D_2O ($\nu_{\mathrm{OD}(\mathrm{D_2O})} = 2316\,\mathrm{cm^{-1}}$) ice Ih at 246 K, which yields $\alpha = 0.738$. Considering a Morse oscillator at this temperature, $\nu_\mathrm{S}^{\mathrm{H_2O}}$ should be

[5] These experiments only yield results for the Γ-point.

reduced more strongly compared to its value at 0 K than $\nu_{\mathrm{S}}^{\mathrm{D_2O}}$. Since temperature effects are neglected in Eq. (6.9), it is thus not surprising that the measured relative frequency shift is underestimated. On the other hand, measurements at 0 K should yield

$$\frac{\partial \nu_{\mathrm{S}}^{\mathrm{D_2O}}}{\partial P} \approx \frac{\partial (\alpha \nu_{\mathrm{S}}^{\mathrm{H_2O}})}{\partial P} \approx 0.728 \cdot \frac{\partial \nu_{\mathrm{S}}^{\mathrm{H_2O}}}{\partial P} \tag{6.10}$$

for the shift of the intramolecular stretching mode peak in the D_2O-isotopologue of ice Ih.

6.5 References

1. V. Fuentes-Landete, S. Rasti, R. Schlögl, J. Meyer, T. Loerting, *J. Phys. Chem. letters* **11**, 8268–8274 (2020).
2. E. R. Pounder, *The physics of ice* (Elsevier, 2013).
3. K. Röttger, A. Endriss, J. Ihringer, S. Doyle, W. F. Kuhs, *Acta Cryst. B* **50**, 644–648 (1994).
4. A. D. Fortes, *Acta Cryst. B* **74**, 196–216 (2018).
5. C. P. Herrero, R. Ramírez, *J. Chem. Phys.* **134**, 094510 (2011).
6. R. Ramírez, N. Neuerburg, M.-V. Fernández-Serra, C. P. Herrero, *J. Chem. Phys.* **137**, 044502 (2012).
7. B. Pamuk, J. M. Soler, R. Ramírez, C. P. Herrero, P. W. Stephens, *et al.*, *Phys. Rev. Lett.* **108**, 193003 (2012).
8. K. Umemoto, E. Sugimura, S. de Gironcoli, Y. Nakajima, K. Hirose, *et al.*, *Phys. Rev. Lett.* **115**, 173005 (2015).
9. K. Umemoto, R. M. Wentzcovitch, *Jpn. J. Appl. Phys.* **56**, 05FA03 (2017).
10. M. A. Salim, S. Y. Willow, S. Hirata, *J. Chem. Phys.* **144**, 204503 (2016).
11. B. Minceva-Sukarova, W. F. Sherman, G. R. Wilkinson, *J. Phys. C: Solid State Phys.* **17**, 5833–5850 (1984).
12. É. D. Murray, G. Galli, *Phys. Rev. Lett.* **108**, 105502 (2012).
13. A. H. Larsen, J. J. Mortensen, J. Blomqvist, I. E. Castelli, R. Christensen, *et al.*, *J. Phys.: Condens. Matter* **29**, 273002 (2017).
14. J. L. Abascal, C. Vega, *J. Chem. Phys* **123**, 234505 (2005).
15. S. Habershon, T. E. Markland, D. E. Manolopoulos, *J. Chem. Phys* **131**, 024501 (2009).
16. S. Plimpton, *J. Comput. Phys.* **117**, 1–19 (1995).
17. P. Ren, J. W. Ponder, *J. Phys. Chem. B* **107**, 5933–5947 (2003).
18. M. L. Laury, L.-P. Wang, V. S. Pande, T. Head-Gordon, J. W. Ponder, *J. Phys. Chem. B* **119**, 9423–9437 (2015).
19. J. W. Ponder *et al.*, *TINKER: Software tools for molecular design*, 2004.
20. K. T. Wikfeldt, E. R. Batista, F. D. Vila, H. Jónsson, *Phys. Chem. Chem. Phys.* **15**, 16542–16556 (2013).
21. V. Babin, G. R. Medders, F. Paesani, *J. Chem. Theory Comput.* **10**, 1599–1607 (2014).
22. V. Babin, C. Leforestier, F. Paesani, *J. Chem. Theory Comput.* **9**, 5395–5403 (2013).
23. G. R. Medders, V. Babin, F. Paesani, *J. Chem. Thoery Comp.* **9**, 1103–1114 (2013).
24. J. P. Perdew, K. Burke, M. Ernzerhof, *Phys. Rev. Lett.* **77**, 3865–3868 (1996).
25. V. Blum, R. Gehrke, F. Hanke, P. Havu, V. Havu, *et al.*, *Comp. Phys. Comm.* **180**, 2175–2196 (2009).

26. V. Havu, V. Blum, P. Havu, M. Scheffler, *J. Comput. Phys.* **228**, 8367–8379 (2009).
27. B. Santra, J. Klimeš, A. Tkatchenko, D. Alfè, B. Slater, *et al.*, *J. Chem. Phys.* **139**, 154702 (2013).
28. J. Sun, R. C. Remsing, Y. Zhang, Z. Sun, A. Ruzsinszky, *et al.*, *Nat. Chem.* **8**, 831–836 (2016).
29. S. Rasti, J. Meyer, *J. Chem. Phys.* **150**, 234504 (2019).
30. D. R. Hamann, *Phys. Rev. B* **55**, R10157–R10160 (1997).
31. P. Vinet, J. R. Smith, J. Ferrante, J. H. Rose, *Phys. Rev. B* **35**, 1945–1953 (1987).
32. A. Togo, I. Tanaka, *Scripta Mater.* **108**, 1–5 (2015).
33. K. Parlinski, Z. Q. Li, Y. Kawazoe, *Phys. Rev. Lett.* **78**, 4063–4066 (1997).
34. K. Lejaeghere, G. Bihlmayer, T. Bjorkman, P. Blaha, S. Blugel, *et al.*, *Science* **351**, aad3000 (2016).
35. G. R. Medders, V. Babin, F. Paesani, *J. Chem. Theory Comput.* **10**, 2906–2910 (2014).
36. C. H. Pham, S. K. Reddy, K. Chen, C. Knight, F. Paesani, *J. Chem. Thoery Comp.* **13**, 1778–1784 (2017).
37. M. Gupta, R Mittal, B. Singh, S. Mishra, D. Adroja, *et al.*, *Physical Review B* **98**, 104301 (2018).
38. K. Umemoto, R. M. Wentzcovitch, *Phys. Rev. B* **69**, 180103 (2004).
39. P. J. Feibelman, *Phys. Chem. Chem. Phys.* **10**, 4688–4691 (2008).
40. J. G. Brandenburg, T. Maas, S. Grimme, *J. Chem. Phys.* **142**, 124104 (2015).
41. Y. Liu, L. Ojamäe, *J. Phys. Chem. B* **120**, 11043–11051 (2016).
42. H. J. Monkhorst, J. D. Pack, *Phys. Rev. B* **13**, 5188–5192 (1976).
43. J. J. Neumeier, *J. Phys. Chem. Ref. Data* **47**, 033101 (2018).
44. B. Santra, J. Klimeš, D. Alfè, A. Tkatchenko, B. Slater, *et al.*, *Phys. Rev. Lett.* **107**, 185701 (2011).